Evaluation of a Filtered Model for the Simulation of Large Scale Bubbling and Turbulent Fluidized Beds

Schalk Cloete[1], Stein Tore Johansen[2] & Shahriar Amini[2*]

1) Department of Energy and Process Technology, NTNU, Trondheim, Norway.

2) Department of Process Technology, SINTEF Materials and Chemistry, Trondheim, Norway.

*Corresponding author. Email: shahriar.amini@sintef.no

Address: SINTEF Materials and Chemistry, Richard Birkelands Vei 3, 7034 Trondheim, Norway.

Phone: +47 46639721

Keywords: Filtered model; Fluidized bed; Large scale; Clusters; Modelling; CFD.

1. Abstract

Full 3D flow simulations of lab and industrial scale dense fluidized beds were carried out using a filtered Eulerian-Eulerian approach. Filtered closures for interphase momentum exchange, solids stresses and additional wall corrections were implemented in the standard equations of motion. These closures had a very large effect on overall model performance when solved on the large cell sizes required for computationally affordable 3D fluidized bed simulations. Numerical experiments conducted under different fluidization conditions showed that the current model formulation performs well over a wide range of operating conditions. It was found that additional modelling accounting for flow non-uniformity is essential under certain fluidization conditions. The current method for dealing with flow non-uniformity by means of wall corrections yielded good results under vigorous fluidization, but caused a slight inaccuracy at low fluidization velocities. In general, comparisons to a wide range of experimental data showed good quantitative agreement, suggesting that the formulation of the filtered model is highly generic. The filtered approach was also successfully verified in a large scale bubbling fluidized bed reactor by comparisons with a highly computationally expensive, well resolved, non-filtered flow simulation.

2. Introduction

Fluidized bed reactors form an integral part of many process industries in operation today. The intimate inter-phase contact and excellent mixing achieved by these reactors offer a highly favourable environment for any gas-solid or solid catalysed reaction. Fluidized bed reactor performance is very difficult to predict, however, primarily due to the complex and highly interconnected physical phenomena involved. Intricate gas-solid hydrodynamics is tightly coupled to heat transfer and heterogeneous reaction kinetics, presenting a distinctly non-linear modelling problem.

The fundamental flow modelling framework of computational fluid dynamics (CFD) is therefore an ideal candidate for accurately modelling these complex reactors. Simultaneous conservation of mass, momentum, energy and species throughout space and time ensure that the non-linear interactions between all relevant physical phenomena are simulated directly. For this reason, CFD modelling of fluidized beds have enjoyed significant research attention over the past two decades. An Eulerian-Eulerian multiphase flow modelling framework closed by the kinetic theory of granular flows (KTGF) [1-3] is regularly used for this purpose.

Another complicating characteristic of fluidized bed reactors is the formation of mesoscale structures (bubbles in bubbling beds and clusters in risers). The size, shape and nature of these mesoscale structures largely determine the behaviour of a fluidized bed and have to be accounted for in order to correctly predict reactor performance [4]. Generally, however, these controlling structures occur on very small time and length scales, requiring fine grids and small timesteps to resolve accurately. A standard Eulerian-Eulerian KTGF approach can therefore only simulate relatively small-scale 2D fluidized beds and a fully resolved, 3D simulation of an industrial fluidized bed is far beyond the capabilities of today's computational facilities.

In order to attain accurate solutions on computational grids coarse enough to allow for large-scale 3D simulations, a filtered approach may be used where the effects of mesoscale structures, now being smaller than the grid size, are modelled based on averaged values of local flow variables. Such an approach allows for computational speedups of several orders of magnitude, but additional closure relations are required to close the filtered conservation equations.

This work is based on filtered two-fluid models of gas-particle flows as formulated by Sundaresan and co-workers [5, 6]. The models were developed in two stages. Firstly, highly resolved simulations of two-fluid models were carried out in periodic domains. The resulting flow-fields were subsequently filtered to obtain filtered constitutive models for fluid-particle drag coefficient, the particle phase pressure and particle phase viscosity. The resulting models depended only on particle and fluid physical properties, particle volume fraction and the filter size. Secondly, highly resolved simulations in a wall-bounded domain were carried out in order to derive the required corrections in near-wall regions.

This approach was demonstrated to achieve good results in riser flows of Geldart A particles [7], but has not been thoroughly evaluated for application in dense bubbling and turbulent fluidized beds. These flow regimes will be the focus of the current study and will present a thorough test for the generality of the current modelling approach. If good results can be attained for a wide range of bubbling and turbulent fluidization cases in addition to the aforementioned favourable riser flow results, it can be interpreted as a very positive result for the filtered modelling approach as it stands now and serve to encourage both academia and industry to further develop this approach. A good generic agreement should encourage academia to extend this approach to also include species, energy and reaction kinetic filtering and encourage industry to start employing and testing this approach in real-world problems involving reactor hydrodynamics. Such an increased focus would significantly accelerate the development of a model capable of making real contributions to industrial fluidized bed reactor design and operation.

Two bed configurations will be considered in the present work: a lab-scale fluidized bed filled with Geldart A particles and operated in the bubbling and turbulent regimes as well as an industrial scale bubbling fluidized bed filled with large Geldart D particles. 3D simulation of the hydrodynamics in these beds lies beyond the capacities of present computational resources, implying that a filtered approach is mandatory for achieving sufficiently accurate numerical solutions.

3. List of Symbols

α Volume fraction

Δ_f Filter length (m)

λ Bulk viscosity (kg/(m.s))

μ Shear viscosity (kg/(m.s))

ρ Density (kg/m^3)

$\bar{\bar{\tau}}$ Stress tensor (kg/(m.s^2))

$\vec{\upsilon}$ Velocity vector (m/s)

∇ Gradient or Del operator (1/m)

C_D Drag coefficient

c Drag filter coefficient

d Diameter (m)

Fr_f Filter size Froude number

$\vec{g}$ Gravity vector (m/s^2)

$h(\alpha_s)$ Scaling function

$\bar{\bar{I}}$ Identity tensor

K Momentum exchange coefficient (kg/(m^3.s))

p Pressure (Pa)

Re Reynolds number

t Time (s)

V Volume (m^3)

$\mathrm{v_t}$ Terminal particle velocity (m/s)

x Distance from the wall (m)

Subscripts:

d Dimentionless

g Gas

p Not filtered (i.e. on a particle level, not on a cluster level)

sg Inter-phase

s Solids

4. Simulations

Numerical simulations will be based on a multiscale modelling approach proposed by Igci *et al.* [5]. In this approach, filtered closures are derived from small scale, well resolved simulations.

4.1 Model equations

The equation system is based on the Eulerian-Eulerian multiphase flow modelling approach, where the two participating phases (gas and solids) are treated as inter-penetrating continua or fluids. This approach is often referred to as the two fluid model (TFM).

4.1.1 Conservation equations

Mass and momentum are conserved for each phase individually.

$$\frac{\partial}{\partial t}\left(\alpha_g \rho_g\right) + \nabla \cdot \left(\alpha_g \rho_g \vec{\upsilon}_g\right) = 0 \qquad (1)$$

$$\frac{\partial}{\partial t}\left(\alpha_s \rho_s\right) + \nabla \cdot \left(\alpha_s \rho_s \vec{\upsilon}_s\right) = 0 \qquad (2)$$

$$\frac{\partial}{\partial t}\left(\alpha_g \rho_g \vec{\upsilon}_g\right) + \nabla \cdot \left(\alpha_g \rho_g \vec{\upsilon}_g \vec{\upsilon}_g\right) = -\alpha_g \nabla p + \nabla \cdot \bar{\bar{\tau}}_g + \alpha_g \rho_g \vec{g} + K_{sg}\left(\vec{\upsilon}_s - \vec{\upsilon}_g\right) \qquad (3)$$

$$\frac{\partial}{\partial t}\left(\alpha_s \rho_s \vec{\upsilon}_s\right) + \nabla \cdot \left(\alpha_s \rho_s \vec{\upsilon}_s \vec{\upsilon}_s\right) = -\alpha_s \nabla p - \nabla p_s + \nabla \cdot \bar{\bar{\tau}}_s + \alpha_s \rho_s \vec{g} + K_{gs}\left(\vec{\upsilon}_g - \vec{\upsilon}_s\right) \qquad (4)$$

In the above equations, all variables represent filtered values.

Since this is only a hydrodynamic study, no conservation of energy or species are included.

4.1.2 Closures

Standard hydrodynamic simulations of fluidized beds are generally closed by the KTGF, modelling subgrid motions of particles on grids much larger than the particle size. In addition to modelling particle scale phenomena, the filtered approach also models mesoscale phenomena by accounting for the presence of subgrid particle structures. Simulations can therefore be carried out on grid sizes larger than the subgrid structures. Filtered closures are added on top of the KTGF closures so that, when no filtering is required, the KTGF closure is used. The KTGF will not be presented in detail here, however, since it is not the primary focus of the study and is well documented in numerous other works (e.g. [4, 8]).

The equation setup used in this paper was receive through personal communication directly from Sundaresan and co-workers and represents the latest and most accurate formulations according to the filtering methodology outlined in two recent publications [5, 6]. While a previous study [7] validated these formulations in riser flows, this study aims to carry out validation studies in the bubbling and turbulent fluidization regimes, thereby fully assessing the generality of the modelling approach.

The first filtered closure is that of interphase momentum transfer $\left(K_{sg} = K_{gs}\right)$ in equations (3) and (4). This is done by modifying the subgrid drag law for the particle [9] by a factor between zero and one. The momentum interaction coefficient is therefore reduced to account for the larger amount of slip experienced by a conglomerate of particles.

$$K_{sg} = K_{sg,p}\left(1+c\right) \tag{5}$$

$$K_{sg,p} = \frac{3}{4} C_D \frac{\alpha_s \alpha_g \rho_g \left|\vec{\upsilon}_s - \vec{\upsilon}_g\right|}{d_s} \alpha_g^{-2.65} \tag{6}$$

$$C_D = \frac{24}{\alpha_g \operatorname{Re}_s}\left[1+0.15\left(\alpha_g \operatorname{Re}_s\right)^{0.687}\right] \tag{7}$$

$$c = -\frac{Fr_f^{-1.6}}{Fr_f^{-1.6}+0.4} h\left(\alpha_s\right) \tag{8}$$

The coefficient c is a function of the filter size, expressed as an inverse Froude number

$$Fr_f^{-1} = g\Delta_f \Big/ \mathrm{v}_t^2 \tag{9}$$

where the filter length is twice the grid size

$$\Delta_f = 2V_{cell}^{1/3} \tag{10}$$

and a scaling function, $h(\alpha_s)$.

$$h(\alpha_s) = \begin{cases} 2.7\alpha_s^{0.234}, \ \alpha_s < 0.0012 \\ -0.019\alpha_s^{-0.455} + 0.963, \ 0.0012 \le \alpha_s < 0.014 \\ 0.868\exp(-0.38\alpha_s) - 0.176\exp(-119.2\alpha_s), \ 0.014 \le \alpha_s < 0.25 \\ -4.59\times10^{-5}\exp(19.75\alpha_s) + 0.852\exp(-0.268\alpha_s), \ 0.25 \le \alpha_s < 0.455 \\ (\alpha_s - 0.59)(-1501\alpha_s^3 + 2203\alpha_s^2 - 1054\alpha_s + 162), \ 0.455 \le \alpha_s \le 0.59 \\ 0, \ 0.59 < \alpha_s \le 0.65 \end{cases} \tag{11}$$

The interphase momentum transfer is therefore modified as a function of the grid size, the particle terminal velocity and the local filtered volume fraction. A physical understanding of the model can be gained by plotting the degree of filtering of the interphase momentum exchange (the bracketed term (1+c) in equation (5)) as a function of the solids volume fraction and the inverse Froude number (equation (9)). This plot is shown in Figure 1.

It is clear that the degree of filtering increases with the inverse Froude number (scaled filter length). This is understandable since a larger filter length (i.e. a coarser grid) implies that less flow detail can be resolved and more modelling is required. The response to volume fraction can also be understood from physical arguments. At the extreme filtered volume fractions of 0 and 0.6, no filtering is required since no clusters can form. It is only in between these two extremes where significant local volume fraction segregation can occur and interphase momentum exchange can be reduced. Figure 1 shows that the effect of clustering on interphase momentum exchange is strongest at relatively low filtered volume fractions and then gradually reduces as the filtered volume fraction increases.

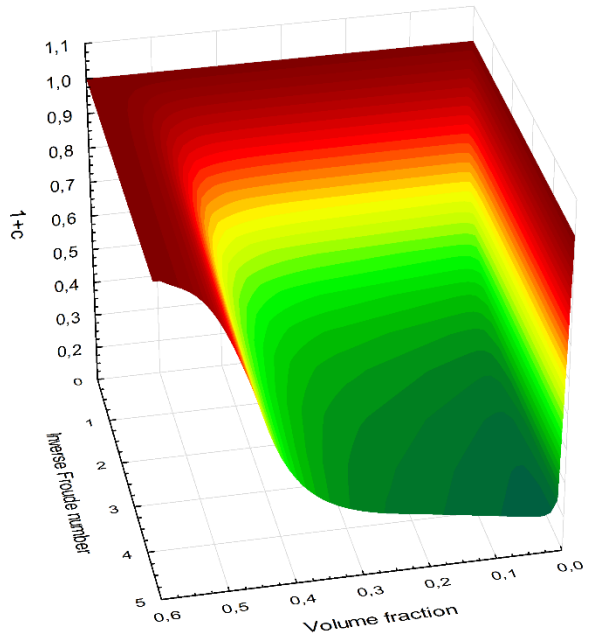

Figure 1: The filtering of the interphase momentum exchange coefficient as a function of particle volume fraction and inverse Froude number.

Secondly, the solids stresses are also modified. Particle structure formation has a diffusive influence on momentum transfer and will therefore be modelled as a stress increase. The solids stress tensor in equation (4) is written as follows:

$$\overline{\overline{\tau}}_s = -\nabla p_s + \alpha_s \mu_s \left(\nabla \vec{\upsilon}_s + \nabla \vec{\upsilon}_s^T \right) + \alpha_s \left(\lambda_s - \frac{2}{3} \mu_s \right) \nabla \cdot \vec{\upsilon}_s \overline{\overline{I}} \tag{12}$$

Three modelled quantities are needed to close this equation: the solids pressure, the shear viscosity and the bulk viscosity. Bulk viscosity is generally small and will be neglected in this study. The solids pressure is modelled as follows:

$$\frac{p_s}{\rho_s \mathrm{v}_\mathrm{t}^2} = \begin{cases} \dfrac{p_{s,p}}{\rho_s \mathrm{v}_\mathrm{t}^2} + Factor_{ps} \left(\alpha_s - 0.59 \right) \left(-1.69 \alpha_s - 4.61 \alpha_s^2 + 11 \alpha_s^3 \right), \ \alpha_s \le 0.59 \\ \dfrac{p_{s,p}}{\rho_s \mathrm{v}_\mathrm{t}^2}, \ \alpha_s > 0.59 \end{cases} \tag{13}$$

$$Factor_{ps} = 0.48 \left(Fr_f^{-0.86} \right) \left(1 - \exp\left(-\frac{Fr_f^{-1}}{1.4} \right) \right) \tag{14}$$

The solids pressure resulting from subgrid motions on the scale of the particles is modelled from the KTGF [1]. Within the filtered approach, this value is not very important, however, since the filtered pressure can easily become three orders of magnitude greater than the KTGF pressure.

The shear viscosity is modelled as follows:

$$\frac{\mu_s g}{\rho_s \mathrm{v_t}^3} = \begin{cases} \frac{\mu_{s,p} g}{\rho_s \mathrm{v_t}^3} + Factor_{\mu s}\left(\alpha_s - 0.59\right)\left(-1.22\alpha_s - 0.7\alpha_s^2 - 2\alpha_s^3\right), \ \alpha_s \le 0.59 \\ \frac{\mu_{s,p} g}{\rho_s \mathrm{v_t}^3}, \ \alpha_s > 0.59 \end{cases} \tag{15}$$

$$Factor_{\mu s} = 0.37 Fr_f^{-1.22} / \left(0.28 Fr_f^{-0.43} + 1\right) \tag{16}$$

Solids shear viscosity on the particle scale is again modelled from the KTGF [3].

Finally, some experimental near wall treatment is employed which reduces the values of all three filtered quantities as the wall is approached.

$$K_{sg,eff} = K_{sg} / \left(1 + 6.0 \exp\left(-0.4 x_d\right)\right) \tag{17}$$

$$p_{s,eff} = p_s / \left(1 + 9.1 \exp\left(-0.45 x_d\right)\right) \tag{18}$$

$$\mu_{s,eff} = \mu_s / \left(1 + 5.6 \exp\left(-0.15 x_d\right)\right) \tag{19}$$

The dimensionless normal distance to the wall used in the wall correction equations is calculated as follows:

$$x_d = xg / \mathrm{v}_t^2 \tag{20}$$

4.2 Geometry, boundary conditions and materials

Two separate geometries were simulated in this study: a lab scale 0.267 m ID fluidized bed and an industrial 5 m ID reactor. The small scale reactor was simulated for comparison with detailed experimental data reported by Zhu *et al.* [10, 11]. This reactor was 2.5 m in height and with an added freeboard region expanding to a height of 4.2 m and an inner diameter of 0.667 m to stop excessive particle entrainment out of the bed. The freeboard region was included in the simulation domain to accurately account for the large degree of bed expansion observed in some of the simulations conducted. The large scale reactor was simulated for comparison to industrial pressure drop data reported in Gobin *et al.* [12]. This reactor was 30 m in height, but 15 m was

found to be sufficient for accurate modelling due to limited bed expansion. The geometries are displayed in Figure 2.

The geometries were meshed with structured hexahedral cells. Cells were maintained close to perfect cubes and the size did not vary discernibly throughout the domain, except in the freeboard region of the lab scale reactor. In some fine grid simulations, only the region where the bed resides was refined by means of hanging node refinement as illustrated for the industrial geometry in Figure 2.

Gas was injected though a velocity inlet on the bottom face of each reactor. Different velocities were used for the lab scale reactor, while the industrial scale reactor injected gas at a velocity of 0.5 m/s. Gas exited at the top of the reactor though a pressure outlet at 0 Pa gauge pressure. A no-slip boundary condition was specified at the walls for the gas phase, while a partial slip boundary condition was specified for the solids. The model of Johnson and Jackson [13] was used for the solids boundary condition with a specularity coefficient of 0.001 describing the wall roughness. This value depends on the reactor material and particle properties and is therefore not known. The low value given above indicates an almost free slip boundary condition and was found to give acceptable results in the current case. This remains an area of significantly uncertainty, however, and could conceivably be responsible for some degree of error in the simulations.

A fine Geldart A [14] powder was used in the lab scale reactor with a density of 1780 kg/m^3 and a mean diameter of 65 μm [10]. Standard air at room temperature was used as the fluidizing gas. The industrial scale reactor contained very coarse Geldart D type particles; density 850 kg/m^3 and mean diameter 1.3 mm. The fluidization gas was pressurized hydrocarbons with a density of 20 kg/m^3 and a viscosity of 1.5e-5 Pa.s [12]. The maximum packing limit was set to 0.63.

Figure 2: The lab scale (left) and the industrial (right) geometries and meshes used in the current study.

4.3 Solver settings

The commercial CFD package, FLUENT 13.0 was used as the flow solver to carry out the simulations. The phase-coupled SIMPLE algorithm [15] was selected for pressure-velocity coupling, while the QUICK scheme [16] was employed for discretization of all remaining equations. 1st order implicit temporal discretization was used.

4.4 Operation and data extraction

The lab scale fluidized bed was initialized as being filled to a height of 0.9 m at maximum packing (volume fraction of 0.63), while the large scale reactor was initialized with a volume fraction of 0.35 up to a height of 8 m. Each simulation was run until a quasi-steady state was reached. This state was identified by monitoring the mass weighted average solids velocity and

observing when this value started fluctuating around a fixed mean. Sampling of time-statistics was subsequently commenced for a minimum of 15 s in the lab scale reactor and 30 s in the industrial scale reactor.

5. Results and discussion

Four sets of numerical experiments were performed. The first, and most comprehensive, was a thorough grid independence and validation study in the lab scale reactor run with Geldart A particles over three different fluidization velocities. Secondly, the generality of the model was evaluated over a wide range of fluidization velocities spanning the bubbling and turbulent fluidization regimes. Thirdly, the relative importance of the various constituents of the filtered model approach was determined. And finally, the filtered approach was applied to a large scale reactor filled with Geldart D particles.

5.1 Numerical experiment 1: Grid independence and detailed validation

Three distinctly different fluidization velocities were considered to investigate model behaviour under different operating conditions: 0.06 m/s (gentle bubbling) 0.4 m/s (vigorous bubbling) and 0.9 m/s (turbulent). Results from each of these flow scenarios will be presented and discussed separately below.

5.1.1 Gentle bubbling – 0.06 m/s

The first case investigated was conducted at a fluidization velocity just high enough to create isolated bubbles rising through the domain. These bubbles do not possess enough buoyancy to create a steady recirculatory flow pattern within the bed. There is thus not any significant radial segregation of volume fraction or velocity within this bed, offering a fairly simple validation case for simulation comparisons.

Firstly, however, grid independence has to be established. This was done for cases run both with and without the wall correction treatment as illustrated in Figure 3.

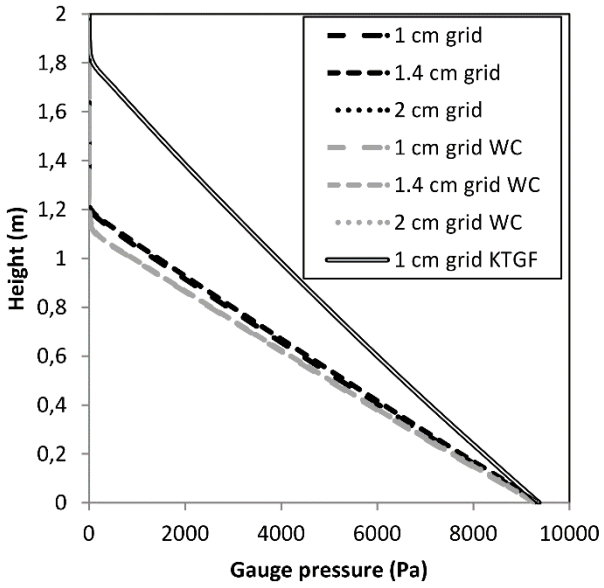

Figure 3: Time averaged axial pressure profiles collected for different grid sizes and model setups at a fluidization velocity of 0.06 m/s. WC indicates the activation of wall corrections and KTGF indicates a non filtered approach closed only by the kinetic theory of granular flows.

It is shown that both the cases with and without the wall corrections achieved fully grid independent results for all three grid sizes investigated. The importance of filtering, even in this case where only a limited number of mesoscale structures were formed is also clearly illustrated by a significant over-expansion of the bed when no filtering is applied.

Figure 3 also suggests that the cases with and without the wall corrections lie very close to each other. This is to be expected since the flow is relatively uniform, meaning that the flow behaviour at the wall is not significantly different from that towards the centre of the reactor and any additional wall treatment should not have a large effect. Comparisons to experimental results are given in Figure 4 and Figure 5.

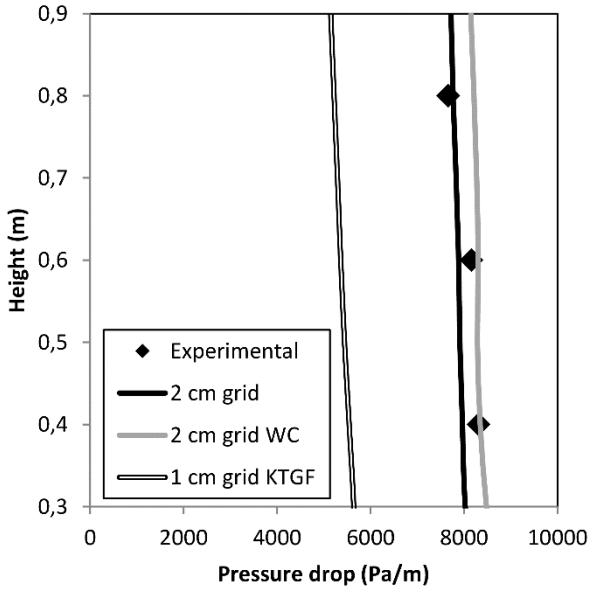

Figure 4: Time averaged axial pressure drop profiles in the lower reactor regions collected for different model setups at a fluidization velocity of 0.06 m/s. WC indicates the activation of wall corrections and KTGF indicates a non filtered approach closed only by the kinetic theory of granular flows. Experimental data was taken from Zhu *et al.* [11].

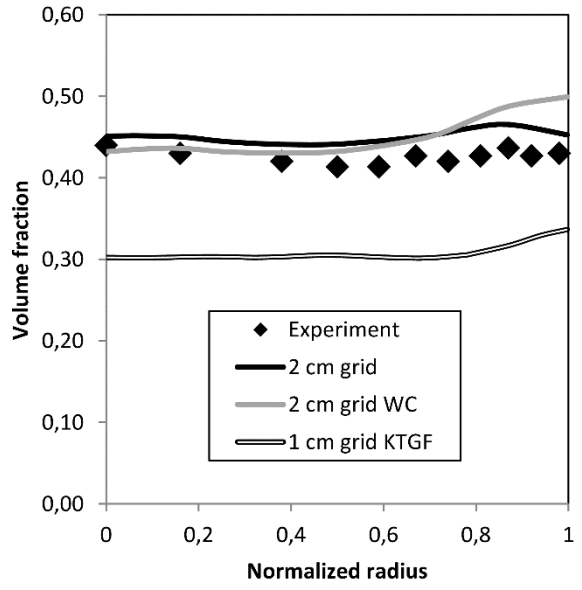

Figure 5: Time averaged radial volume fraction profiles at a height of 0.6 m for the grid independent solutions achieved both with and without activation of the wall corrections for a fluidization velocity of 0.06 m/s. Experimental data was taken from Zhu *et al.* [11].

Both filtered simulations compare well to experiments, whereas the non filtered approach shows substantial discrepancies. The simulation run with the wall corrections shows a small degree of radial volume fraction segregation which is not reflected in the experimental results, but still provides a very reasonable representation of the physics.

It stands to reason that the wall corrections will only be required if the local flow conditions at the wall are significantly different from the local flow conditions in the bulk of the vessel. In this case, however, the flow was virtually uniform throughout the entire vessel and the inclusion of the wall corrections had a marginally negative impact on results. Wall corrections should therefore be formulated to approach zero in the limit of such a slowly fluidized bed.

5.1.2 Vigorous bubbling – 0.4 m/s

The next flow scenario investigated represents freely bubbling fluidization. Here, the typical recirculatory flow pattern expected in bubbling fluidized beds is formed. Bubbles migrate towards the centre of the vessel, causing a strong up-draft in the centre and complimentary down-flow at the walls. Results from the grid independence study for this flow scenario are presented in Figure 6.

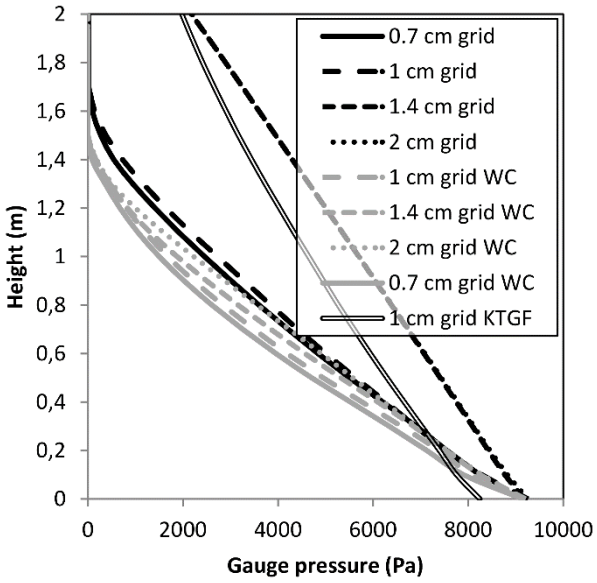

Figure 6: Time averaged axial pressure profiles collected for different grid sizes and model setups at a fluidization velocity of 0.4 m/s. WC indicates the activation of wall corrections

and KTGF indicates a non filtered approach closed only by the kinetic theory of granular flows.

Some rather surprising model behaviour is seen in Figure 6. The simulation with the wall corrections achieved what is essentially a grid independent solution on all grids investigated, but when no wall corrections were included, there was a large and decidedly non-linear dependency on the grid size. Figure 6 shows that, for a grid size of 1.4 cm and above, the bed height is grossly over-predicted, while for a grid size of 1 cm and below, grid independence is suddenly achieved at a much more compact bed. This scenario requires some closer investigation with the aid of Figure 7.

The unexpected grid dependence behaviour is described in the first four columns on the left of Figure 7. A very large change in flow behaviour between a grid size of 1.4 cm and a grid size of 1 cm is clearly visible, corresponding to the pressure profiles reported in Figure 6. For the simulation run on a grid of 1 cm, it is clear that some unsteady flow structures are resolved, while these structures are completely lost on the 1.4 cm grid. This sudden change between these two distinctly different flow scenarios can be explained by considering that such transient flow structures are self-sustaining. The moment that the grid size becomes small enough to resolve the structures, some strong down-flows are resolved next to the walls, the average volume fraction in the bed increases, and structure formation becomes more likely.

The structures which are resolved in the simulations are not the real mesoscale structures (bubbles) which are modelled by the filtered approach, but rather a kind of super-structure consisting of many bubbles. This kind of flow response can be envisioned from the third and fourth columns of Figure 7.

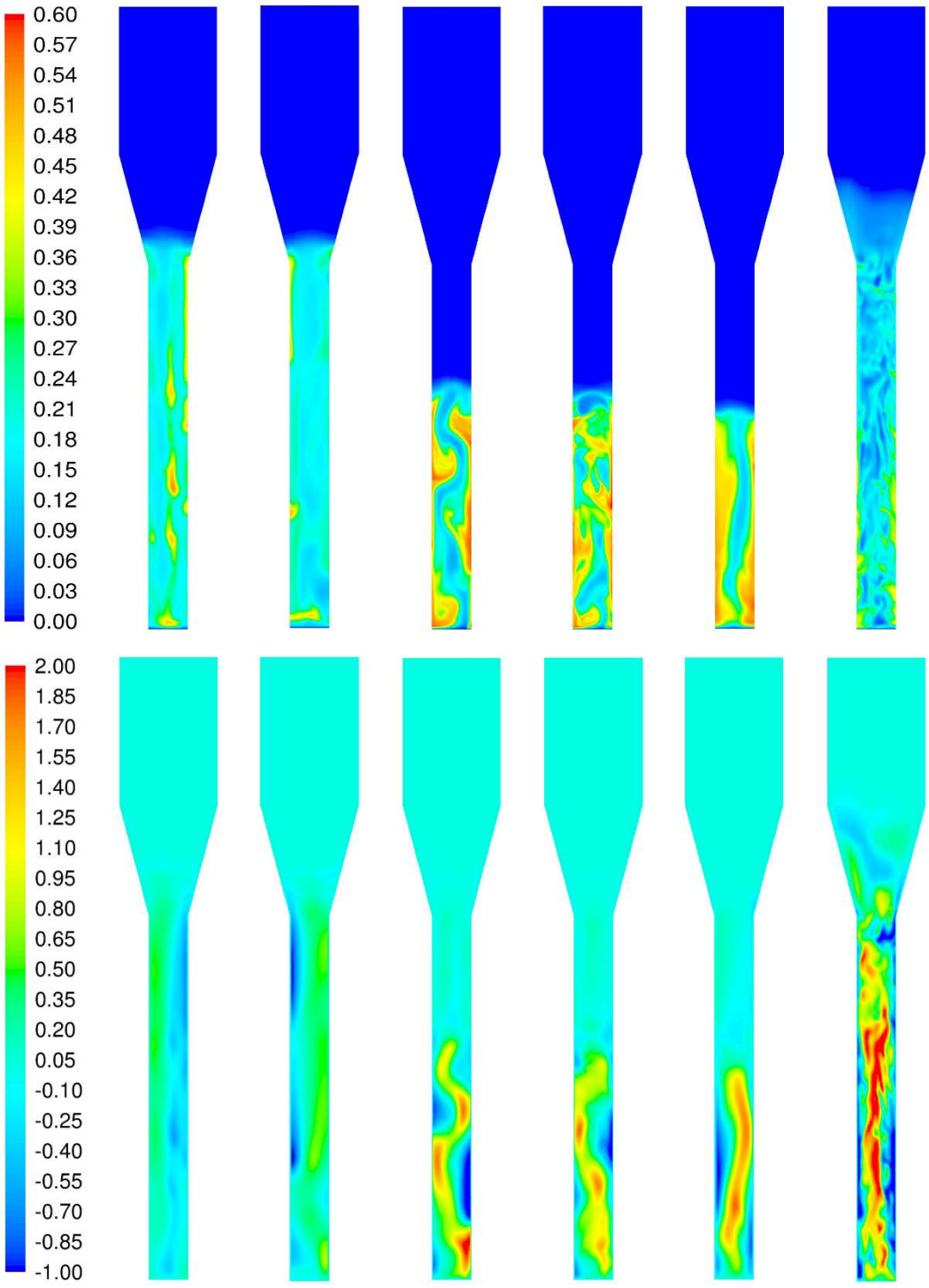

Figure 7: Instantaneous volume fraction (top row) and axial velocity (bottom row, m/s) contours for various model setups. From left to right, the cases represent four runs without

wall corrections on grids of 2 cm, 1.4 cm, 1 cm and 0.7 cm, one case with wall corrections run on a grid of 2 cm and one case without any filtering run on a grid of 1 cm.

The filtered approach used in this study was developed on the assumption that all filtered variables are uniform within each computational cell. Cells containing large gradients in filtered volume fraction or velocity can therefore not be adequately treated using this approach and some additional modelling will be required. An example of such an approach uses a modelled drift velocity based on filtered volume fraction and velocity gradients to account for spatial non-uniformities within the volume of filtering [17]. In the current study, however, these non-uniformities are accounted for by means of the wall corrections. The wall regions in fast moving flows are typically where large gradients in all flow variables occur and localising this additional treatment to the wall regions appears to be reasonable.

The second to last column in Figure 7 shows that the dense down-flows are correctly captured even on a coarse grid when the wall corrections are activated. This can be caused by the drag reduction allowing solids to fall much more easily in the near wall regions or by the reduction in solids stresses allowing greater strain rates and establishing the recirculatory flow pattern typical of bubbling fluidized beds.

Another interesting feature that can be deduced from Figure 7 is that the correct prediction of bed expansion depends just as much on the accurate resolution of solids recirculation as on the accurate modelling of subgrid drag. This can be seen by comparing the first two columns (where subgrid drag is modelled, but no recirculatory flow is achieved) to the last column (where no subgrid drag is modelled, but some degree of recirculation is achieved). Despite the filtered drag model reducing the interphase exchange coefficient by a factor of five, the bed expansions predicted by these two different scenarios are quite similar, implying that, in this particular case, the effect of recirculation is comparable in magnitude to the effect of subgrid drag.

Figure 8 and Figure 9 show the comparison of simulation data to experimental results. The pressure drop profiles (Figure 8) clearly indicate the importance of the wall corrections in this case. The model results with the wall corrections included succeeded in capturing the axial reduction in pressure gradient measured in experiments, while the simulations without wall corrections predicted a more uniform pressure gradient along the bed. This implies that the

increased solids recirculation facilitated by the wall corrections is indeed necessary to correctly capture the denser lower regions of the bed.

For the radial volume fraction profile shown in Figure 9, however, it is shown that the model over-predicts the degree of radial solids volume fraction segregation in the vessel, especially when the wall corrections are activated. The particular experimental case with which the simulations are compared exhibited a large degree of non-symmetry in the flow, even after 30 s of averaging, due to a spiralling bubble motion in the bed [10]. The experimental trend reported in Figure 9 was averaged from three different time averaged radial measurements, one of which differed significantly from the others. This asymmetry is the primary reason for the relatively uniform experimental volume fraction trend shown in Figure 9 and could not be accurately captured by the model. Spiralling bubble motion is a fairly isolated phenomenon, however, and will not be of great interest to industry. A precise simulation match is therefore not of high priority in this case.

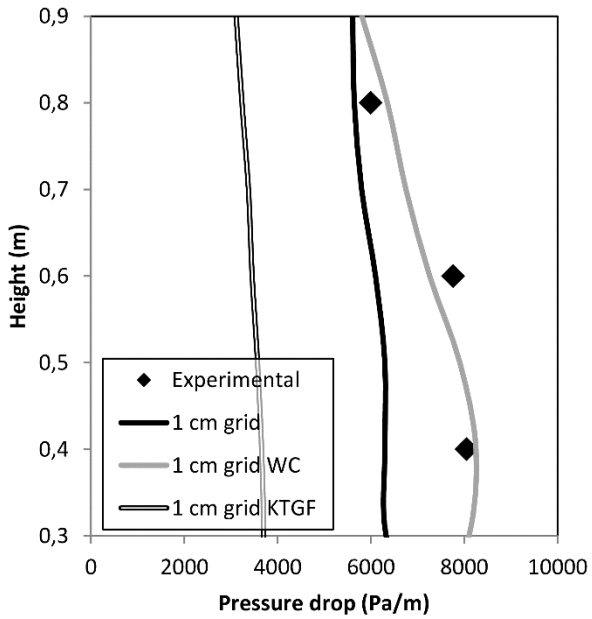

Figure 8: Time averaged axial pressure drop profiles in the lower reactor regions collected for different model setups at a fluidization velocity of 0.4 m/s. WC indicates the activation of wall corrections and KTGF indicates a non filtered approach closed only by the kinetic theory of granular flows. Experimental data was taken from Zhu *et al.* [11].

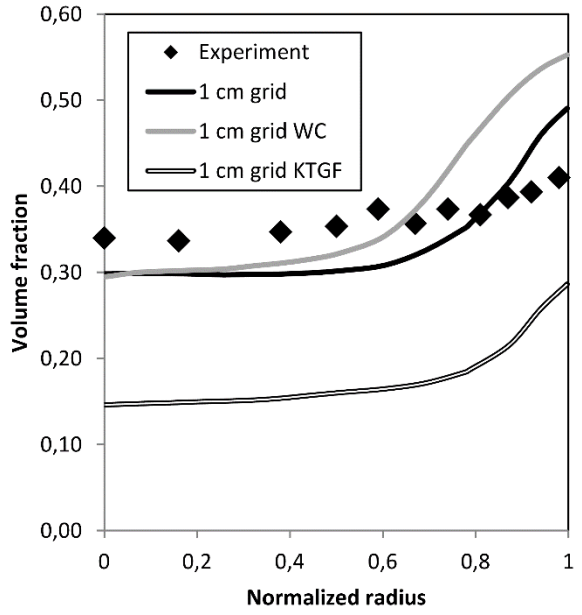

Figure 9: Time averaged radial volume fraction profiles at a height of 0.6 m for the grid independent solutions achieved both with and without activation of the wall corrections for a fluidization velocity of 0.4 m/s. Experimental data was taken from Zhu *et al.* [11].

5.1.3Turbulent bed – 0.9 m/s

The final flow scenario investigated falls in the turbulent fluidization regime. Grid independence results for this case are shown in Figure 10.

Complete grid independence could not be achieved for any of the cases investigated. When the wall functions were activated, however, grid independence behaviour was improved. Differences in pressure predictions solved on the various grids with the wall corrections activated are relatively small and the overall bed expansion solved on all grids is virtually identical. It is also interesting to note that the difference between simulations with and without wall corrections is significantly larger than it was for the previous two cases utilizing a slower fluidization velocity. This is an indication that the high fluidization velocity investigated here causes large strain rates in the regions of the walls that require special treatment to capture correctly.

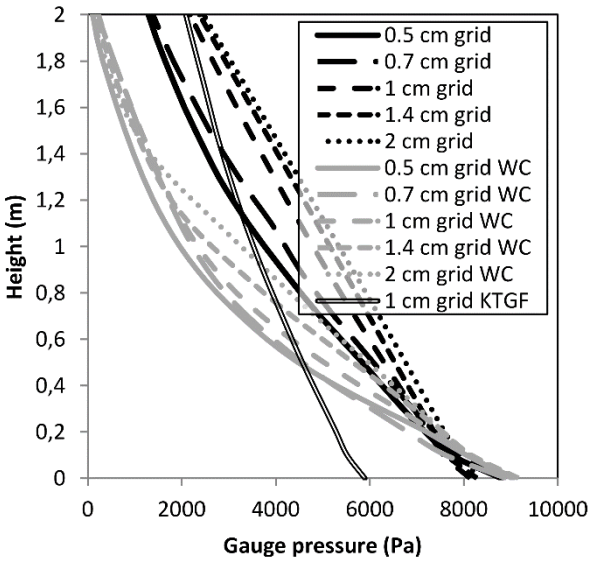

Figure 10: Time averaged axial pressure profiles collected for different grid sizes and model setups at a fluidization velocity of 0.9 m/s. WC indicates the activation of wall corrections and KTGF indicates a non filtered approach closed only by the kinetic theory of granular flows.

The importance of filtering in general is also well demonstrated in Figure 10 and Figure 11 where it can be seen that the bed height will be greatly over-predicted and the pressure gradient under-predicted by a factor of three when no filtering is employed. The significant under-prediction of the total pressure drop over the bed in the case without any filtering is due to a large percentage of solids being fluidized into the freeboard region where solids can rest on the diagonally expanding walls of the geometry (see Figure 2). These solids are therefore not entirely fluidized and do not contribute to the total pressure drop.

Model performance is checked against experimental data in Figure 11 and Figure 12 where a very good qualitative and quantitative fit is reported for the full model. The model without any wall corrections shows an under-prediction of the overall volume fraction due to the significant non-uniformity in the flow.

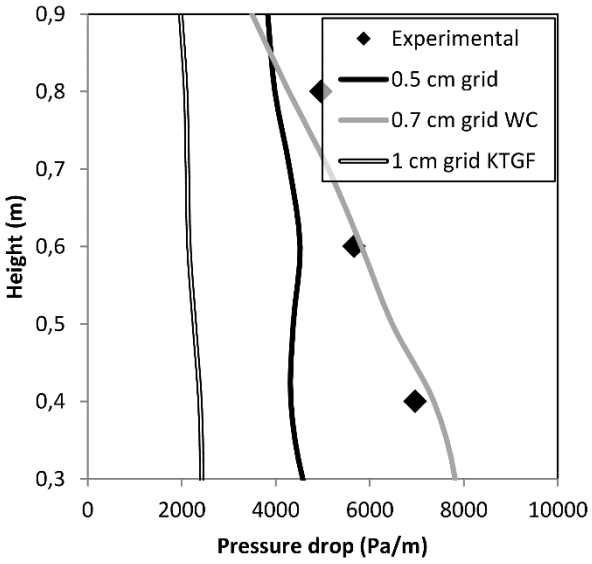

Figure 11: Time averaged axial pressure drop profiles in the lower reactor regions collected for different model setups at a fluidization velocity of 0.9 m/s. WC indicates the activation of wall corrections and KTGF indicates a non filtered approach closed only by the kinetic theory of granular flows. Experimental data was taken from Zhu *et al.* [11].

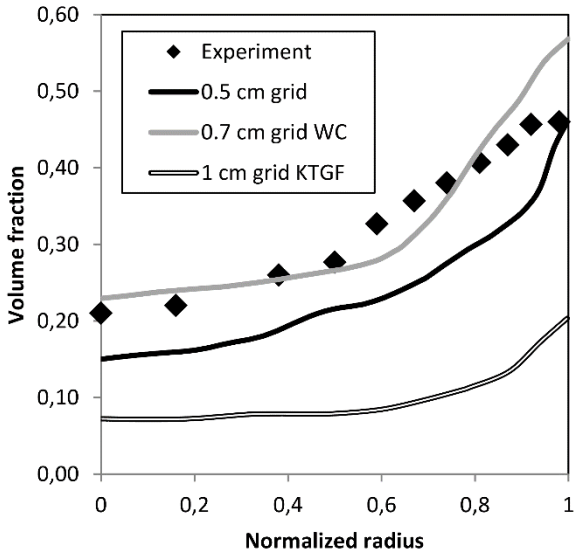

Figure 12: Time averaged radial volume fraction profiles at a height of 0.6 m for the grid independent solutions achieved both with and without activation of the wall corrections for a fluidization velocity of 0.9 m/s. Experimental data was taken from Zhu *et al.* [11].

In order to attain some more detailed information on the inability of the full model to achieve complete grid independence (Figure 10), the axial volume fraction profiles for each of the different mesh sizes investigated were plotted in Figure 13. Here it can be confirmed that the model shows good grid independence behaviour on all the mesh sizes investigated. The primary difference lies in the volume fraction predictions close to the wall, where finer grids seem to cause a slight over-prediction. The strength of the wall corrections increases exponentially towards the wall and finer grid cells close to the wall can better capture this strong effect. In a 3D cylindrical geometry, the wall regions represent a large percentage of the cross sectional area and this over-prediction caused the increase in the axial pressure gradient in the lower region of the vessel when finer grids were used (Figure 10).

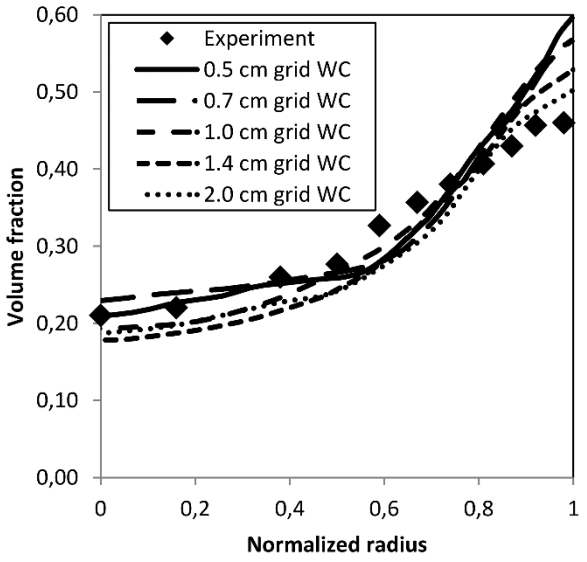

Figure 13: Time averaged radial volume fraction profiles at a height of 0.6 m for different grid sizes with wall corrections included and a fluidization velocity of 0.9 m/s. Experimental data was taken from Zhu *et al.* [11].

5.2 Numerical experiment 2: Generality

Generality is the most important quality measure of any predictive model. Within the fundamental framework of CFD, model generality will depend completely on the formulation of the models used to close the conservation equations. In this case, these models are the filtered closures for interphase momentum exchange, solids stresses and wall corrections.

In order to test the generality, the full model was run over a wide range of fluidization velocities on a grid size of 2 cm, assuming that this grid size grants acceptable grid independence. Results are given in Figure 14.

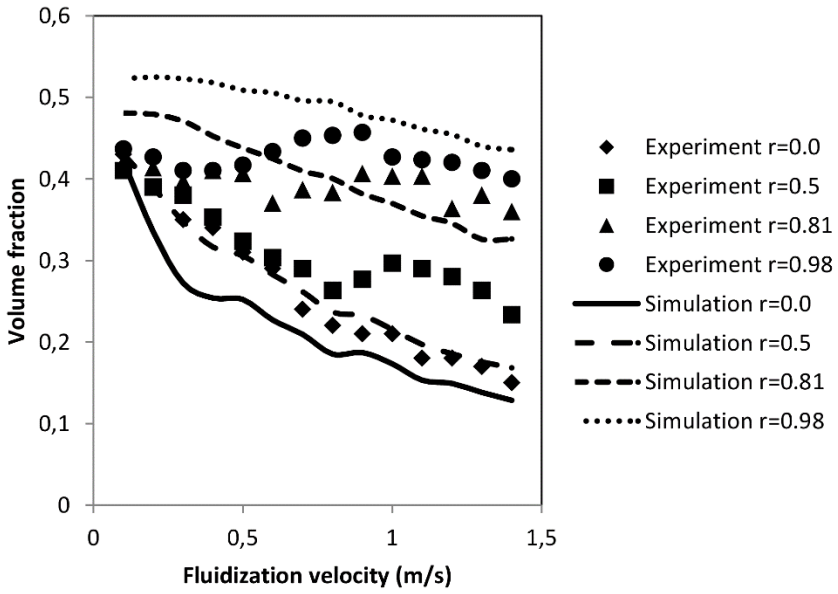

Figure 14: Time averaged solids volume fraction measurements at four normalized radial locations (0, 0.5, 0.81 and 0.98) at a height of 0.6 m over a wide range of fluidization velocities. Experimental measurements were taken from Zhu *et al.* [11].

A reasonable quantitative agreement is seen throughout the wide range of data depicted in Figure 14. In general, the model is shown to under-predict the solids volume fraction in the centre and over-predict it at the walls. The most important feature in Figure 14, however, is that the model shows the expected intuitive trend of volume fraction steadily declining with an increase in fluidization velocity, whereas the experiments show several counter-intuitive volume fraction increases with an increase in fluidization velocity. Under the assumption that the experimental results are correct, this implies that the model fails to capture certain non-linear system effects that are responsible for this counter-intuitive trend. The spiralling bubble motion alluded to in the discussion of Figure 9 is one such non-linear effect.

Still, even though the model does not capture the counter-intuitive trends, the predictions are generally good considering the degree of modelling difficulty of this particular setup. Firstly, the experimental system used very small particles, forming very small and virtually impregnable

structures. This implies that the model performance will be very sensitive to the formulation of subgrid closures and even a small error in the filtered model formulation will influence results. The experimental bed also had a relatively small diameter, implying that the walls greatly influenced overall system behaviour. Walls not only introduce a significant degree of uncertainty in the description of the direct boundary conditions, but also create the recirculating flow pattern which has a very large influence on overall system behaviour. The interaction between the downflows at the walls and the upflows at the centre of the vessel is highly complex and very sensitive to model formulation, especially in a narrow bed. In addition, the bubbling and turbulent fluidization regimes considered typically involve a large degree of flow segregation, both in terms of volume fraction and velocity, just adding to the sensitivity of the modelled system. A number of effects that could have a significant effect were also neglected, primarily the particle size distribution and molecular inter-particle forces. When considering these challenges, the predictions in Figure 14 are certainly quite reasonable.

Industrial bubbling and turbulent fluidized beds will generally involve larger particles and have much larger diameters than the lab-scale system considered here. These two factors will greatly simplify the modelling problem and it is safe to say that model performance will improve in such systems. The greater simplicity of these systems should also prevent counter-intuitive system performance trends (such as those shown in Figure 14) and the inability of the model to correctly capture these trends will not be a major limitation.

5.3 Numerical experiment 3: Parametric study

The full filtered model, including the wall corrections, performed well in the case of turbulent fluidization (0.9 m/s fluidization velocity) on a rather coarse 2 cm grid. In order to test the importance of the various constituent models in the filtered approach, this simulation was repeated with specific constituent models deactivated. The results are plotted in Figure 15 and Figure 16.

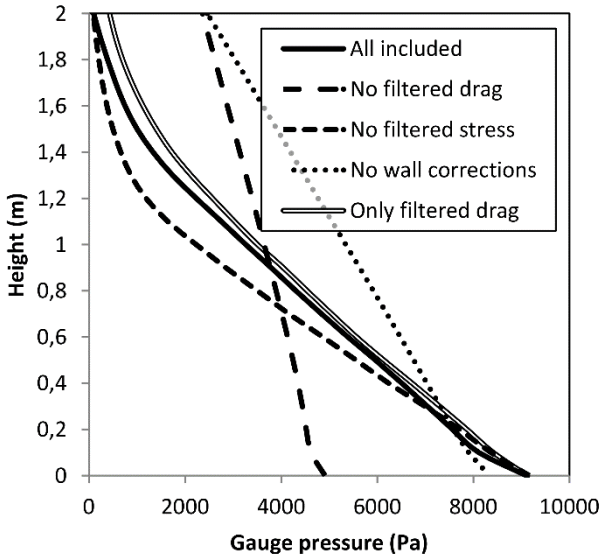

Figure 15: Time averaged axial pressure profiles collected for different model setups at a fluidization velocity of 0.9 m/s.

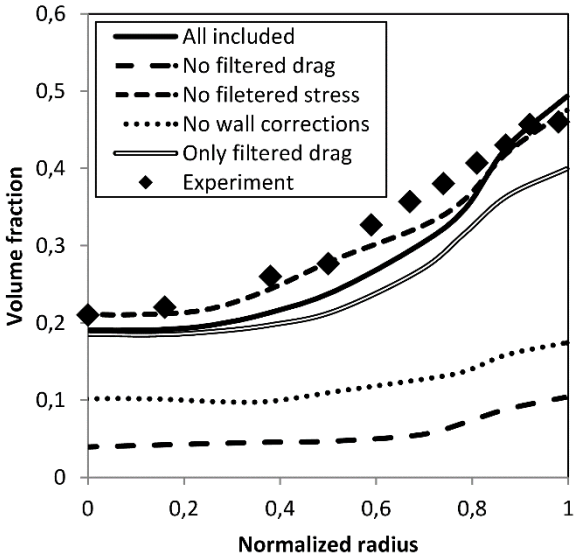

Figure 16: Time averaged radial volume fraction profiles at a height of 0.6 m collected for different model setups at a fluidization velocity of 0.4 m/s.

The filtered approach consists of three major constituent models: interphase momentum transfer, solids stresses and wall corrections. Figure 15 and Figure 16 show that the deactivation of interphase momentum transfer and wall corrections has a highly significant effect on model performance. In both cases the bed expansion is greatly over-predicted. When the filtered drag is

deactivated, this is simply due to an over-prediction of interphase momentum exchange. When the wall corrections are deactivated, however, the excessive bed expansion is due to the recirculating flow pattern not being successfully established.

When looking at the 'No filtered stress' case in Figure 15 and Figure 16, it would appear that the deactivation of solids stresses only has a small impact on the results. However, when the wall corrections are deactivated, a significant effect of the filtering of the solids stresses becomes visible. This can be seen by comparing the 'No wall corrections' case with the 'Only filtered drag' case. Filtering results in a several orders of magnitude increase in the solids stresses, and thereby prevents the rapid strain rates necessary to facilitate the recirculatory flow pattern. It seems that the deactivation of filtered solids stresses, albeit unphysical, actually results in fairly good model predictions simply because it allows for correct flow recirculation, similar to the effect of the wall corrections.

A closer investigation into the behaviour of the wall corrections was also undertaken by alternatively deactivating the drag and stress constituents. These results are displayed in Figure 17 and Figure 18.

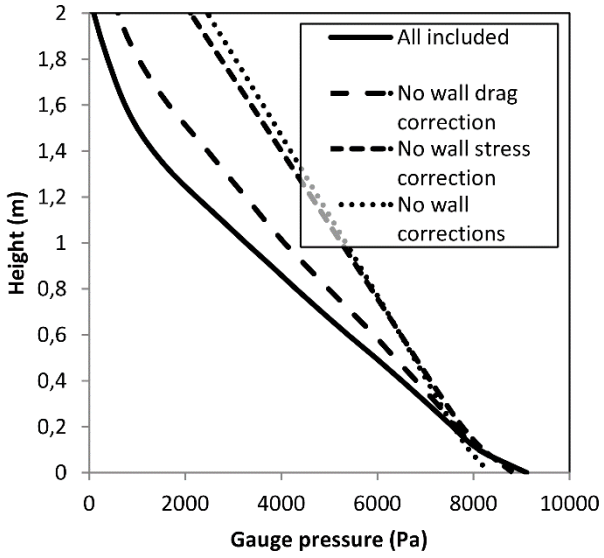

Figure 17: Time averaged axial pressure profiles collected for different wall correction setups at a fluidization velocity of 0.9 m/s.

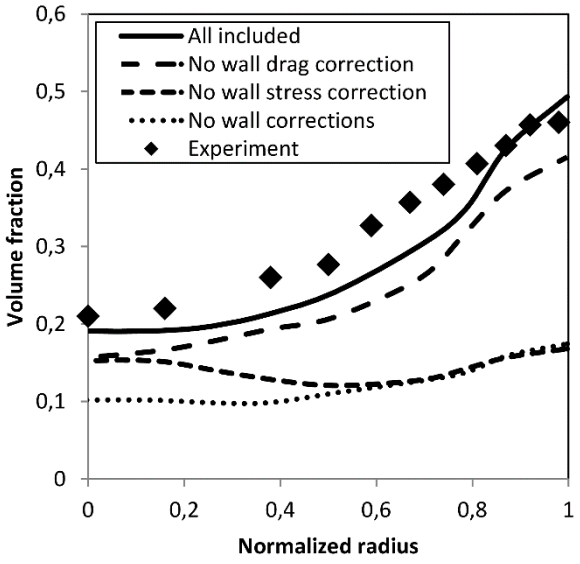

Figure 18: Time averaged radial volume fraction profiles at a height of 0.6 m collected for different wall correction setups at a fluidization velocity of 0.4 m/s.

Results clearly identify the solids stresses as the dominant component in the wall function formulation. Deactivation of the drag term had a comparatively small influence on results. The wall functions therefore facilitate the establishment of a recirculating flow in the reactor by reducing the solids stresses at the wall and allowing the rapid strain rates required by the recirculating flow.

5.4 Numerical experiment 4: Large scale reactor

Naturally, the ultimate aim of any filtered approach is to enable the simulation of large scale systems. Therefore, the present approach was tested in an industrial scale reactor in order to evaluate its applicability to this ultimate purpose.

Industrial scale reactor data is rarely published and can be unreliable. The experimental values of pressure drop used for experimental comparison in this study were estimated from the data reported in Gobin *et al.* [12]. Only two pressure measurements were available in the large scale reactor, one at a height of 3.5 m and the other at a height of 6.5 m. The pressure drop between them was experimentally measured to be between 9 and 11 kPa. An average of 10 kPa will be taken. Some more detailed pressure drop measurements were made in a pilot scale unit scaled to one third of the industrial one. These points confirmed a virtually linear pressure drop profile

along the height of the reactor. From these data, a linear pressure drop of 3333 Pa/m can be deduced. The total pressure drop over the reactor can be estimated from the weight of the solids that has to be fluidized as 23348 Pa. An estimated linear pressure profile can therefore be specified with a gradient of 3333 Pa/m and a y-intercept of 23348 Pa. Numerical simulations will be compared against this experimental estimation.

Firstly, simulations were carried out with the filtered and non-filtered approaches on grid sizes that would typically be used to run computationally efficient simulations of large-scale fluidized bed reactors. Results are reported in Figure 19.

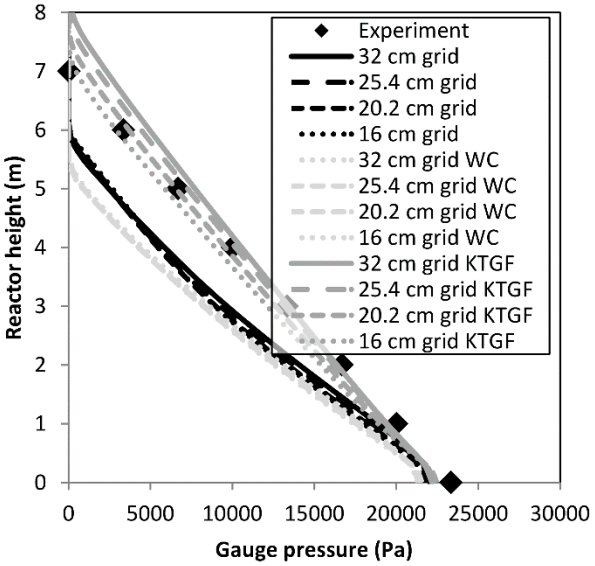

Figure 19: Axial time averaged pressure profiles for simulations with different coarse grid sizes performed with the filtered model closures both with and without the wall corrections (WC) and the non-filtered approach (KTGF).

It is clear that significant grid dependence effects exist for the non-filtered approach, while the filtered approach displays suitable grid independence. The difference between the filtered and the non-filtered results is significantly smaller than that reported for the lab scale bed (Figure 6 and Figure 10). This is due to the large difference in the particle sizes used in the two reactors. When a Geldart A powder is used, mesoscale particle structures quickly become virtually impregnable to the fluidizing gas due to the very large surface area presented by the tiny particles within the structure. This implies that the drag interaction changes completely when such

impregnable structures are formed. As observed in Ellis *et al.* [18], the solution becomes virtually independent of the particle drag formulation in this type of flow as the interphase momentum transfer is completely dominated by cluster formation. For very large particle sizes such as the Geldart D particles considered here, significant slip exists between individual particles and the fluidizing gas. The formation of particle clusters in these flows does add to the degree of interphase slip, but not to such a large extent as observed for the Geldart A class. Thus, fluidization of Geldart A powders can be considered to be exclusively structure dominated, while fluidization of Geldart D powders is controlled by drag interactions both on a particle and structure level. Since only a particle drag law is included in non-filtered simulations, coarse grid simulations of Geldart A powders will fail completely, while similar simulations of Geldart D powders might still be reasonable.

In such a large reactor (5 m ID), conventional wisdom says that wall effects should be negligible, but results show that the wall corrections still had a small, but significant effect on the overall bed expansion. The wall correction approach was only tested for particle sizes up to 100 μm and the very large particle size considered here could lie well outside the range of model validity. For very large particle sizes, the high terminal velocity significantly reduces the normalized distance from the wall (equation (20)) and greatly increases the distance from the wall over which the wall corrections still have an influence. Figure 20 shows that, 1 m in from the wall, the wall corrections still cause close to a factor of 2 decrease in the interphase momentum exchange coefficient.

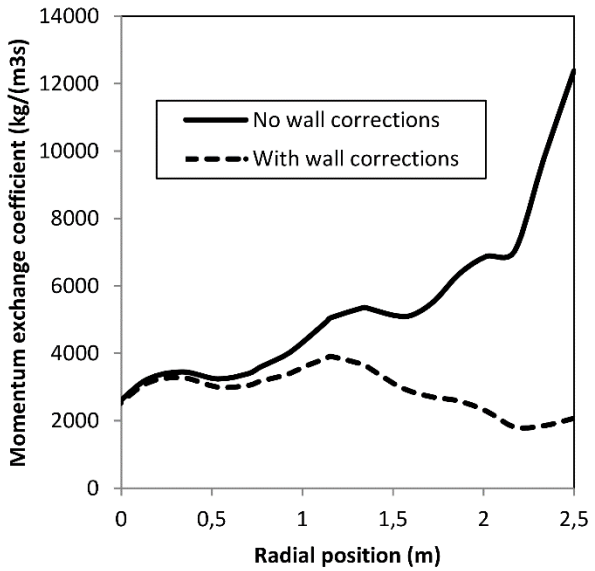

Figure 20: Instantaneous radial profile of the filtered interphase momentum exchange coefficient at a height of 5 m as modeled with and without the wall corrections.

Another observation that can be made from Figure 19 is that the filtered approach predicts a denser bed than that estimated from the experimental results. The predicted bed height is approximately 14% lower than the experimental estimate when no wall functions are included and 24% lower when wall functions are included. This difference could very well be explained by uncertainties in the estimation of the experimental trend or the model setup. Also note that the predicted pressure gradient in the upper regions of the bed, where the experimental measurements were taken, is virtually identical to the experimental measures. It is only in the lower regions of the bed where the simulated pressure drop increases, indicating that the assumption of a linear pressure drop profile might not have been correct.

In order to further test whether the filtered approach is valid, some additional fine grid simulations were completed in order to test whether well resolved and filtered simulations would return the same solution. These results are reported in Figure 21.

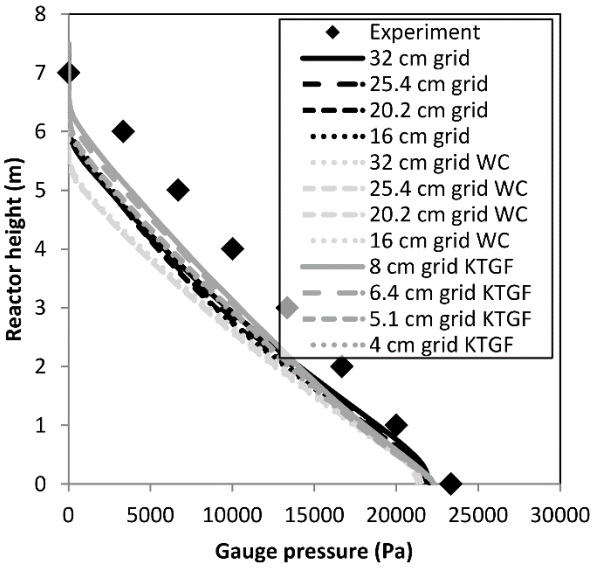

Figure 21: Axial time averaged pressure profiles for filtered and resolved (KTGF) simulations performed on different grid sizes.

It is shown that the resolved simulations displayed a small amount of grid dependence up to a 4 cm grid beyond which further simulations were not possible due to computational constraints. The resolved simulations appear to agree better with the simulations completed without the activation of the wall corrections, but it is possible that the use of even smaller cells could move the resolved simulation results closer to filtered results with wall corrections included.

To get further insight, the mean flow statistics were analysed to determine whether the inclusion of the wall corrections improved the results. As shown in Figure 22, this appears to be the case since the mean flow patterns in the bed become highly asymmetric when the wall corrections are excluded. When the wall corrections are included, on the other hand, the flow patterns match very closely to those in the resolved simulation.

Therefore, despite the very large effect of the wall corrections discussed in Figure 20, it appears that the inclusion of these corrections is essential to correctly capture the flow patterns inside the vessel. If the wall corrections are not included, the narrow region of down-flow at the wall is not captured and the bed material circulates in a highly asymmetric way. Therefore, even though the inclusion of the wall corrections may cause a slight over-compaction of the bed, these corrections are mandatory to correctly capture the physics occurring within the reactor.

In addition, it should also be acknowledged that this case (bubbling fluidization with Geldart D particles) falls far outside the range for which the filtered models were originally developed (riser flows with Geldart A particles). It can therefore be concluded that scaling via the Froude number (equation (9)) and the dimensionless wall distance (equation (20)) is sufficiently generic.

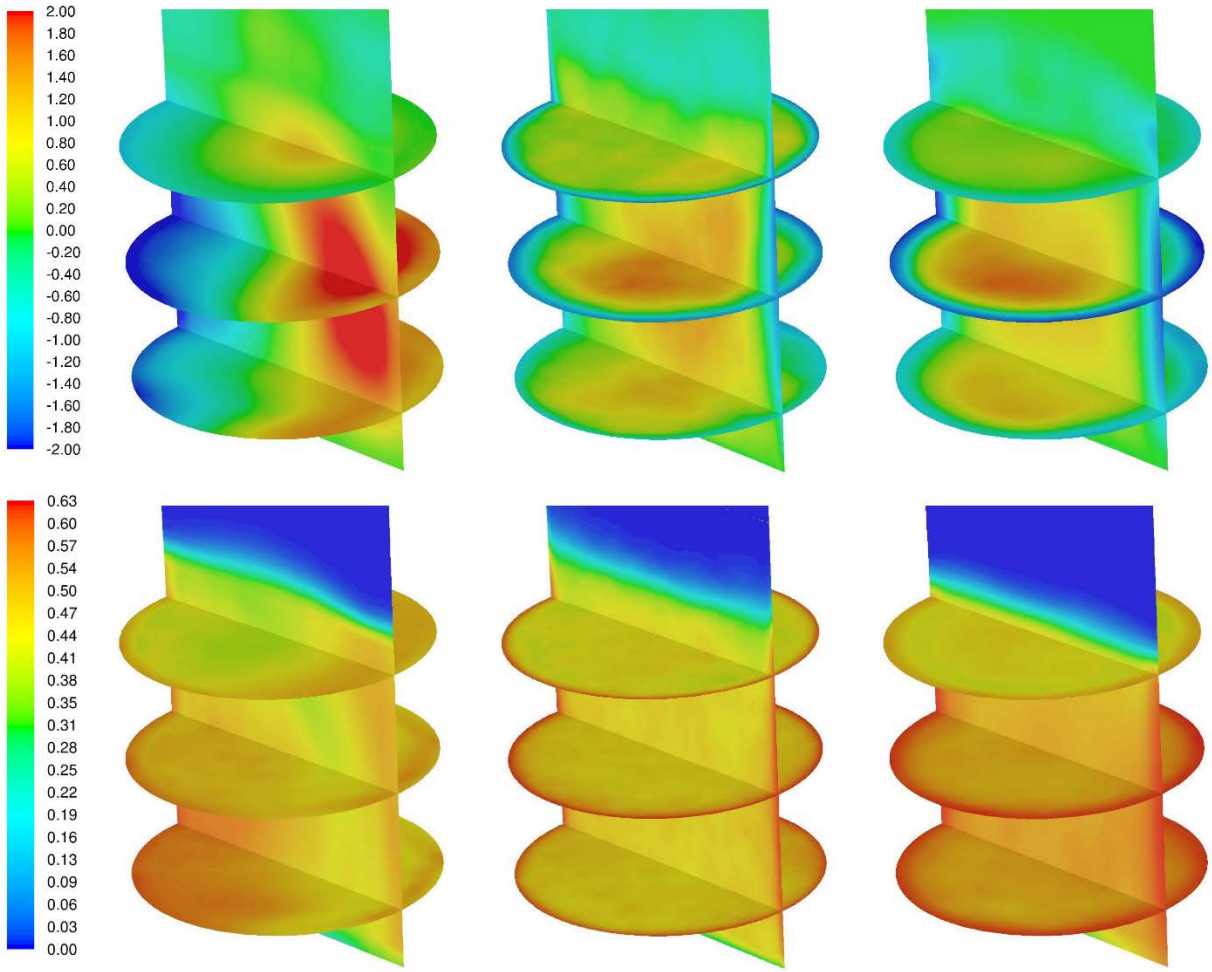

Figure 22: Time-averaged solids vertical velocity (top row) and volume fraction (bottom row) for the filtered case without wall corrections and with 16 cm cells (left) the resolved case with 4 cm cells (centre) and the filtered case with wall corrections and 16 cm cells (right).

6. Conclusions

A multiscale filtered approach for modelling large scale dense fluidized beds has been evaluated. Using this approach, the effects caused by subgrid mesoscale structure formation were modelled in terms of three filtered quantities: the interphase momentum exchange, the solids stresses and additional wall corrections.

When applied to a fine, Geldart A powder, filtering had a very large impact on model performance. Mesoscale structures originating in this type of powder completely dominate interphase momentum transfer and have to be accounted for either by well resolved simulations or by filtering. In addition, the macroscopic recirculatory flow patterns also have to be correctly captured in order to accurately predict bed behaviour. In fact, simulations showed that the correct capturing of solids recirculation is just as important as correct modelling of local interphase momentum transfer.

Flow situations characterized by strong recirculation exhibit large radial non-uniformities in filtered volume fraction and velocity. Wall corrections were used to account for non-uniformity in the flow and caused significant improvements in model performance for situations where significant flow recirculation was present. The activation of wall corrections also allowed grid independent solutions to be attained on much coarser grids. Wall corrections were therefore found to be an important and highly beneficial addition to filtered modelling.

Simulations conducted over a wide range of fluidization velocities spanning bubbling and turbulent fluidization also showed reasonable quantitative comparisons between simulation and experiment. Some distinctly non-linear effects present in the experimental data were not adequately captured by the model, but it was reasoned that these isolated effects were not of major concern. In general, the model was shown to give adequate replications of the flow over a very wide range of operating conditions.

The filtered approach was also applied to a large scale reactor containing coarse, Geldart D type particles. Filtering had a significant effect on these simulations as well, but the effect was substantially smaller than that observed for the Geldart A powder. The interphase momentum interaction occurring in such coarse powders is influenced both on the particle scale and on the

structure scale, implying that the simulations neglecting mesoscale structure modelling would still capture some of the physics through the particle drag law employed.

Due to the large particle size employed, it was possible to conduct a sufficiently grid independent, non-filtered simulation of this industrial scale reactor where all mesoscale structures were adequately resolved. The full filtered model showed a slight over compaction in relation to the resolved simulation, but reproduced the macroscopic flow pattern with great accuracy. When the wall corrections were excluded, down-flows next to the walls were not resolved and a highly asymmetric flow pattern developed which did not match with the resolved simulation.

The encouraging model generality reported in this paper suggests that the filtering approach of Sundaresan and co-workers is a very good candidate for further development by filtering the species and energy transport as well as the gas-solid reaction kinetics in the same manner.

7. Acknowledgements

The authors are very grateful for the regular support from Professor Sankaran Sundaresan in order to gain a good fundamental understanding of the filtered approach to fluidized bed modelling and attain the latest formulations of the various closure models employed.

The authors would also like to acknowledge the financial support from the Research Council of Norway as well as the use of the supercomputing facilities at the Norwegian University of Science and Technology for the most expensive simulations carried out in this study.

8. References

[1] Lun CKK, Savage SB, Jeffrey DJ, Chepurniy N. Kinetic Theories for Granular Flow: Inelastic Particles in Couette Flow and Slightly Inelastic Particles in a General Flow Field. Journal of Fluid Mechanics. 1984;140:223-56.

[2] Gidaspow D, Bezburuah R, Ding J. Hydrodynamics of Circulating Fluidized Beds, Kinetic Theory Approach. *7th Engineering Foundation Conference on Fluidization* 1992:75-82.

[3] Syamlal M, Rogers W, O'Brien TJ. MFIX Documentation: Volume 1, Theory Guide. Springfield: National Technical Information Service 1993.

[4] Cloete S, Amini S, Johansen ST. On the effect of cluster resolution in riser flows on momentum and reaction kinetic interaction. Powder Technology. 2011;210(1):6-17.

[5] Igci Y, Andrews AT, Sundaresan S, Pannala S, O'Brien T. Filtered two-fluid models for fluidized gas-particle suspensions. AIChE Journal. 2008;54(6):1431-48.

[6] Igci Y, Sundaresan S. Constitutive Models for Filtered Two-Fluid Models of Fluidized Gas–Particle Flows. Industrial & Engineering Chemistry Research. 2011 2011/12/07;50(23):13190-201.
[7] Igci Y, Pannala S, Benyahia S, Sundaresan S. Validation Studies on Filtered Model Equations for Gas-Particle Flows in Risers. Industrial & Engineering Chemistry Research. 2011 2012/02/01;51(4):2094-103.
[8] Taghipour F, Ellis N, Wong C. Experimental and computational study of gas-solid fluidized bed hydrodynamics. Chemical Engineering Science. 2005;60(24):6857-67.
[9] Wen CY, Yu YH. Mechanics of Fluidization. Chemical Engineering Progress Symposium Series. 1966;62:100-11.
[10] Zhu H, Zhu J, Li G, Li F. Detailed measurements of flow structure inside a dense gas-solids fluidized bed. Powder Technology. 2008;180(3):339-49.
[11] Zhu H. Turbulent Fluidized Bed vs. High Density Riser - Regimes and Flow Characterizations [PhD]: The University of Western Ontario; 2006.
[12] Gobin A, Neau H, Simonin O, Llinas J, Reiling V, Selo J. Fluid dynamic numerical simulation of a gas phase polymerization reactor. International journal for numerical methods in fluids. 2003;43(10-11):1199.
[13] Johnson PC, Jackson R. Frictional-Collisional Contitutive Relations for Granular Materials, with Application to Plane Shearing. Journal of Fluid Mechanics. 1987;176:67-93.
[14] Geldart D. Types of gas fluidization. Powder Technology. 1973;7(5):285-92.
[15] Patankar S. Numerical Heat Transfer and Fluid Flow: Hemisphere Publishing Corporation 1980.
[16] Leonard BP, Mokhtari S. ULTRA-SHARP Nonoscillatory Convection Schemes for High-Speed Steady Multidimensional Flow. NASA TM 1-2568 (ICOMP-90-12); 1990; NASA Lewis Research Center; 1990.
[17] Parmentier J. Extension of the Euler/Euler Formalism for Numerical Simulations of Fluidized Beds of Geldart A Particles; 2010.
[18] Ellis N, Xu M, Lim CJ, Cloete S, Amini S. Effect of Change in Fluidizing Gas on Riser Hydrodynamics and Evaluation of Scaling Laws. Industrial & Engineering Chemistry Research. 2011;50(8):4697-706.